Analog (p,n) cross sections of even-even palladium isotopes at 26 MeV

J. D. Anderson, V. R. Brown, R. W. Bauer, B. A. Pohl, and C. H. Poppe
Lawrence Livermore National Laboratory, University of California, Livermore, California 94550

S. Stamer, E. Mordhorst, and W. Scobel
I. Institut für Experimentalphysik, University of Hamburg, Hamburg, Federal Republic of Germany

S. M. Grimes
Ohio University, Athens, Ohio

V. A. Madsen
Oregon State University, Corvallis, Oregon
(Received 17 November 1989)

The differential cross sections for the (p,n) reaction to the ground-state and first 2^+ excited analogs of the four even palladium isotopes (104, 106, 108, and 110) have been measured at a proton bombarding energy of 26 MeV. Integrated cross sections for the analog states deviate from the linear dependence on neutron excess as was previously found in other sets of isotopes, e.g., the molybdenum and zirconium isotopes. The observed dependence on deformation of the ground-state analog transition is in quantitative agreement with calculations, which include the inelastic couplings originally used to explain the molybdenum results. Detailed ten-coupled-channels calculations including the ground state, the one- and two-quadrupole phonon collectives states in Pd, and their analogs in Ag give excellent agreement simultaneously with proton elastic scattering, proton inelastic scattering to the first 2^+ state, ground-state analog transitions, and 2^+ analog-state transitions. The effect of the one-step isovector deformation was too small to be extracted from these data.

I. INTRODUCTION

In studies of the (p,n) reaction[1-5] the angle integrated isobaric analog cross sections deviated considerably from the Lane-model[6] predictions of near linearity with neutron excess $(N-Z)$. Coupled-channels calculations[7] indicated that this deviation can be explained by couplings to the low-lying collective states and their analogs. These calculations confirmed that the excitation of analogs of strong collective states proceed primarily by two-step mechanisms, the effect of the one-step process being negligibly small.[7] For the 0^+ ground-state analog transition, the dominant one-step amplitude is reduced by the (destructive) addition of three three-step amplitudes that are nearly in phase with each other. Therefore, when the first excited 2^+ states are coupled, for example, the cross section for the 0^+ analog state decreases by an amount that is roughly proportional to the inelastic $(p,p')2_1^+$ cross section. In addition, the 2_1^+ analog transition is roughly proportional to the product of the inelastic $(p,p')2_1^+$ cross section and the 0^+ analog cross section. Such coupled-channels calculations should therefore be performed not only on the basis of (p,n) data but simultaneously for the elastic and inelastic proton scattering to guarantee a consistent description.

Variation of $\sigma/(N-Z)$ from constancy is greatest for nuclei with large deformation parameters. The mass region $A \approx 100$ offers a number of examples of isotope sets with a range of collectivities broad enough to produce large departures from constancy. Our present measurements with 26 MeV projectiles and time-of-flight techniques extends the earlier (p,n) measurements in this mass region on molybdenum and zirconium to the palladium isotopes. The existence of good elastic and inelastic proton scattering cross sections for the Pd isotopes in the literature[8,9] in the same energy region permits detailed quantitative calculations to be performed.

II. EXPERIMENTAL METHOD AND DATA REDUCTION

The experiment was carried out in two separate runs at the Hamburg Isochronous Cyclotron Facility. The energy of the incident proton beam was 25.9 ± 0.1 MeV in the first series of measurements and 26.1 ± 0.1 MeV in the second series. The beam impinged on self-supporting foils of highly enriched ($>93\%$) palladium isotopes 104, 106, 108, and 110 with thicknesses ranging from 4.0 to 9.9 mg/cm^2. A beam burst separation of 829 ns was obtained by effectively ($>99.8\%$) suppressing 15 out of 16 burst with an external deflection system. The resulting beam intensity of approximately 80 nA allowed one set of measurements to be completed within about 4 h with a charge of typically 1 mC accumulated in the heavily shielded Faraday cup. A schematic layout of the beamline together with the target chamber and the neutron

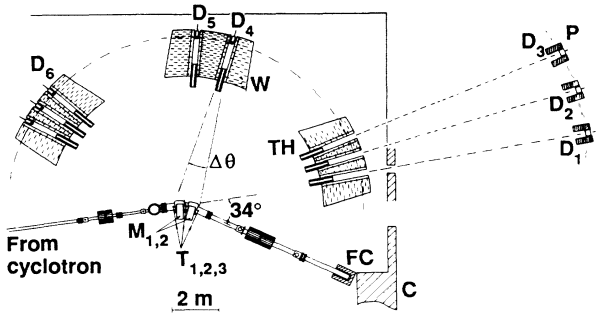

FIG. 1. Schematic diagram of the TOF target positions (T_1, T_2, T_3) and the detector (D_1 through D_8) geometry with water (W), paraffin (P), and concrete (C) shielding, conical polyethylene throats (TH) and bending magnets (M_1, M_2).

time-of-flight setup is shown in Fig. 1.

The standard Hamburg neutron time-of-flight (TOF) setup consists of 8 detectors (10-cm diam × 5-cm deep cylindrical cells filled with liquid scintillator NE 213) and flight paths ranging from 7 to 8 m. The target chamber is surrounded by two bending magnets which produce a total deflection of the beam of 34°. There are three optional target positions, one located in front of the first target magnet, the other between the two target magnets, and the third behind the second target magnet. This arrangement covers the range $3° \leq \theta_{lab} \leq 177°$ with 24 roughly equidistant positions. This experimental setup as well as its performance in the spectroscopy of continuous neutron distributions has been described previously in detail.[10,11]

For the present series of experiments the setup was modified to improve the neutron energy resolution for the angles $\theta_{lab} \leq 60°$. First, the stop signal of the TOF measurement was derived from the dynamically corrected[12] cyclotron radio frequency resulting in a long term burst width of 0.8–1.2 ns (FWHM). Secondly, the TOF paths for the forward detectors D_1, D_2, and D_3 were extended to approximately 20 m (see Fig. 1). These paths were equipped with larger scintillators (25-cm diam × 5-cm deep cylinders of NE 213 or Bicron 501) with individual additional shielding. These upgraded detectors covered the angular positions of 3°, 9°, 15°, 27°, 33°, 47°, and 53° and yielded time resolutions ranging from 1.5 to 2.5 ns. With this setup an overall energy resolution ranging from 125 to 200 keV, depending on the individual detectors and the target thickness, could be expected for the isobaric analog transitions ($E_n \approx 12.5$ MeV).

The detectors were calibrated with threshold energies defined by the 90% point at the Compton edges of several gamma sources and biases set at $E_p = 1.4$ MeV for the short, and 3.2 MeV for the long path detectors. With these settings, n-γ pulse-shape discrimination[10,13] could be applied with a high level of confidence. Data acquisition was performed with standard electronics.

A representative TOF spectrum for a detector at the long flight path is shown in Fig. 2(a). Conversion into absolute energy spectra [Fig. 2(b)] was achieved using time calibrations derived from the position of the gamma peaks from two subsequent beam bursts. The efficiencies were calculated with the code NEFF4.[14] The data from the detectors with the Bicron 501 scintillators required

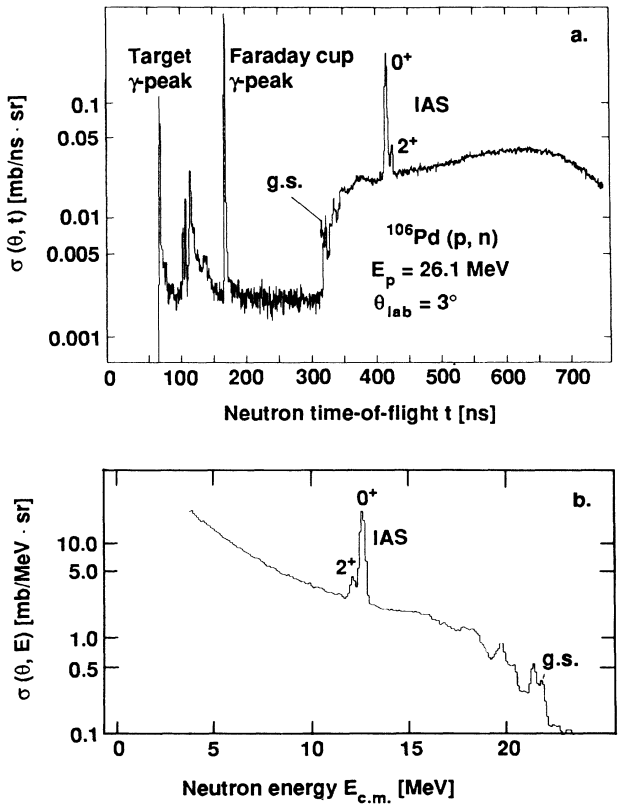

FIG. 2. Representative TOF spectrum (top) and resulting neutron energy spectrum (bottom). Data were taken with 0.45 ns/channel resolution. The transitions to the ground state (g.s.), the 0^+ and 2^+ isobaric analog states (IAS) are indicated.

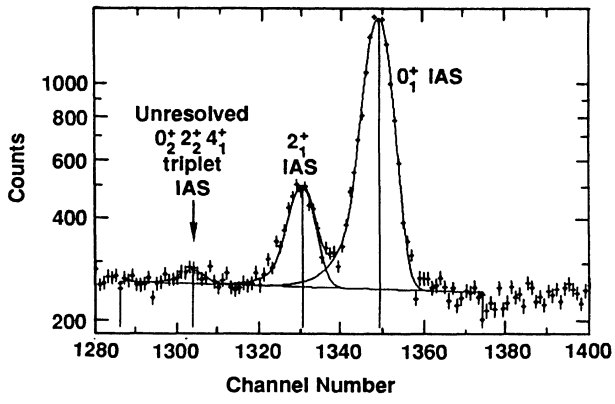

FIG. 3. Example of the ground-state analog peak, first excited-state analog, and two-phonon triplet analog peaks as fitted by the FITEK program. Note that the ordinate is a logarithmic sale, while the abcissa is linear in channels and increasing time is toward the left.

additional corrections because of composition differences and were found to be consistent with those from the NE 213 detectors. The resolutions obtained for the analog states were in agreement with the values anticipated.

The uncertainties resulting from target inhomogeneities and impurities ($<5\%$), incomplete beam current integration ($<3\%$), and detector efficiency ($\leq 4\%$) lead to a minimum uncertainty $\Delta\sigma/\sigma = 7\%$ of the differential cross sections σ. Additional contributions to the uncertainty are due to counting statistics and peak integration (see below).

The characteristic features of the neutron TOF spectra, as seen in Fig. 2, are a number of neutron peaks superimposed on a neutron continuum. The 0^+ ground state analog state is clearly identifiable in all spectra. Kinematic calculations were used to locate the 2_1^+ first excited analog state which was identified in most of the spectra. Kinematics were also used to locate the positions of the unresolved $0_2^+, 2_2^+, 4_1^+$ two-phonon triplet of analog states, which were discernable in all but the most forward and some of the backward angles. In order to determine the counts in the respective peaks the peak-fitting program FITEK was used.[15] This program is highly interactive and is used to define its own peak shape, find the major and minor peaks in a selected spectral range, and fit the peaks as well as the background underneath them. Kinematics were also used to fix the positions of minor

TABLE I. Integrated Pd(p,n) ground-state analog cross sections in mb at 26 MeV. Comparison of experiment with coupled-channels calculations.

Isotope	$(N-Z)$	σ (Expt.)	σ (Calc.)	$\sigma/(N-Z)$ (Expt.)
104	12	3.53±0.25	3.77	0.29±0.02
106	14	3.83±0.27	4.06	0.27±0.02
108	16	3.78±0.26	4.26	0.24±0.02
110	18	4.28±0.30	4.42	0.24±0.02

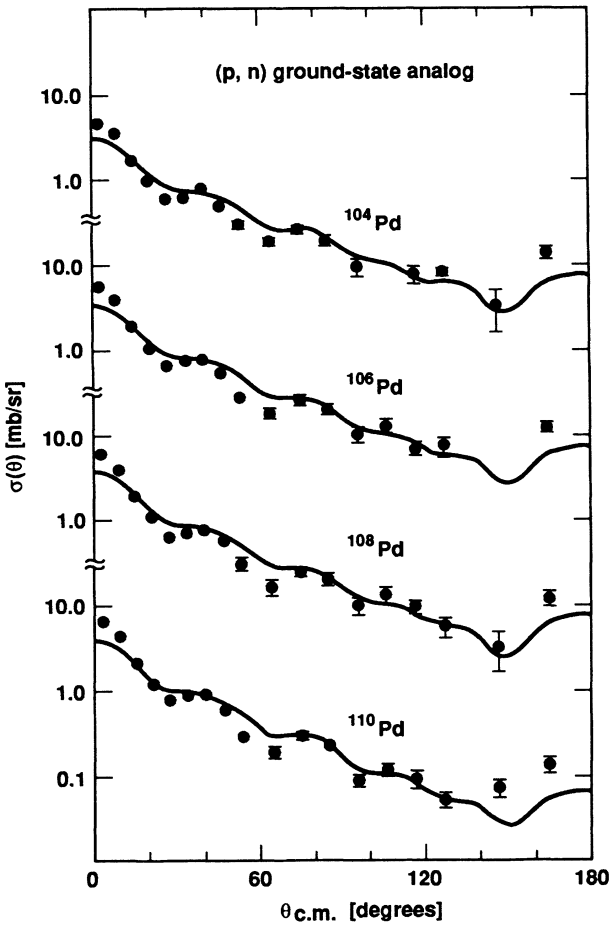

FIG. 4. Angular distributions for the (p,n) reaction to the ground-state analog for the palladium isotopes. The absolute cross sections are shown. The curves represent the coupled-channels calculations.

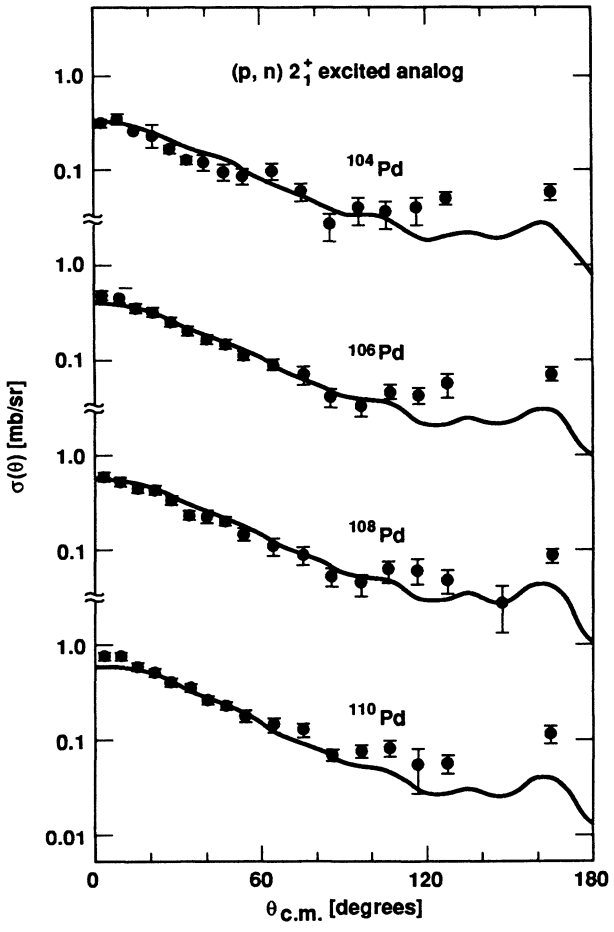

FIG. 5. Angular distributions for the (p,n) reaction to the 2_1^+ first excited-state analog for the palladium isotopes. The absolute cross sections are shown. The curves represent the coupled-channels calculations.

TABLE II. Integrated Pd(p,n) excited-state analog cross sections in mb at 26 MeV. Comparison of experiment with coupled-channels calculations.

Isotope	$\sigma(2_1^+)$[a] (Expt.)	$\sigma(2_1^+)$[a] (Calc.)	$\sigma(0_2^+,2_2^+,4_1^+)$[b] (Expt.)	$\sigma(0_2^+,2_2^+,4_1^+)$[b] (Calc.)
104	0.89±0.06	0.84	0.14±0.03	0.09
106	1.04±0.07	0.99	0.17±0.03	0.11
108	1.32±0.09	1.33	0.25±0.04	0.14
110	1.74±0.12	1.45	0.45±0.05	0.24

[a]Transition to the (2_1^+) first excited analog state.
[b]Transition to the unresolved (0_2^+, 2_2^+, 4_1^+) two-phonon analog triplet.

peaks, such as the 2_1^+ and the two-phonon peaks, with respect to the major peak, the ground-state analog. An example of a FITEK result is given in Fig. 3. The peak shape was found to be a skewed Gaussian with a small tail toward later times (toward lower neutron energies). The integral under the curve determines the sum of the counts in the peak. The uncertainty, also determined by FITEK, includes the statistical error of the signal and background as well as the error due to the deviation of the individual data points from the skewed Gaussian defined by the program. Thus, the total calculated error includes both the statistics and a measure of the goodness of the fit of the Gaussian to the data. This total error was combined with the systematic uncertainty of 7% discussed earlier.

Using the counts in the respective peaks, together with the previously determined detector efficiencies and known target thicknesses, we calculated the differential cross sections for the ground-state analog peak, for the 2_1^+ first excited analog, and for the unresolved two-phonon analog triplet, for the four even palladium targets. Figures 4, 5, and 6 show the respective differential cross sections in the center-of-mass system for the four isotopes. Theoretical results from our coupled-channels calculations, also shown in Figs. 4, 5, and 6 are discussed in Sec. III C.

Each of these angular distributions was fitted with a series of Legendre polynomials in order to determine the integrated cross sections. Errors in the integrated cross sections were determined from both the relative errors in the individual data points and from the goodness of fit of the polynomial series to the data. The results are presented in Tables I and II.

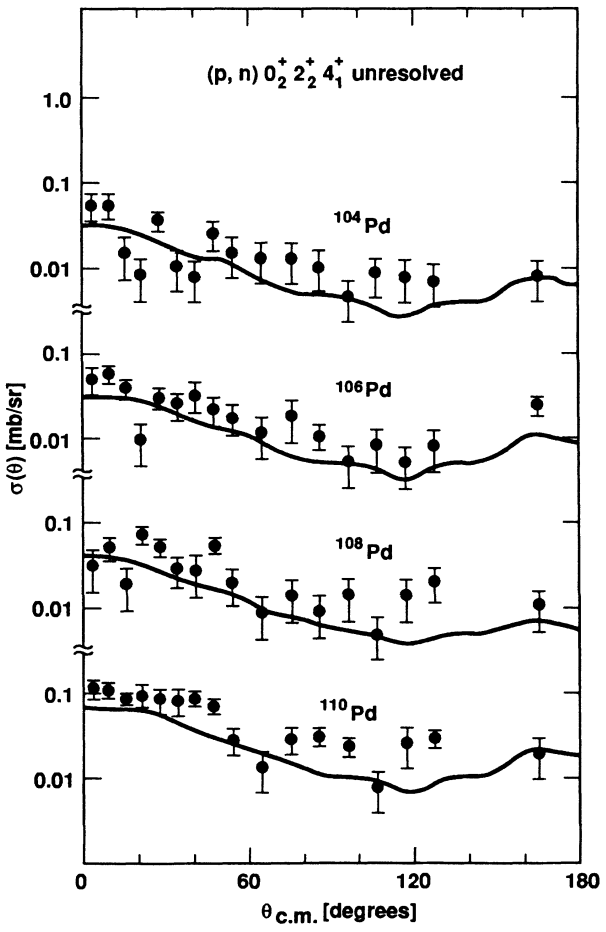

FIG. 6. Angular distributions for the (p,n) reaction to the unresolved ($0_2^+,2_2^+,4_1^+$) two-phonon excited triplet analog for the palladium isotopes. The absolute cross sections are shown. The curves represent the coupled-channels calculations.

III. COUPLED-CHANNELS ANALYSIS AND COMPARISON WITH DATA

A. Optical potential

Our Lane-model optical-potential parametrization is based on the Becchetti-Greenless (BG) "best fit" global proton potential,[16] but uses as its isovector part a modification of a potential due to Patterson *et al.*,[17] hereafter referred to as the MSU (p,n) potential. The criterion for determining an isospin consistent global potential is that it should simultaneously account (at least qualitatively) for (p,p) (p,n) IAS, and (n,n) data. No (n,n) data were available, but we used (p,p) and (p,n) data to determine the following regional Lane optical potential for neutrons and protons, which is utilized for all Pd isotopes and energies discussed:

$$V_R(_n^p) = 53.4 - 0.32E + 0.4zZ/A \pm V_1\epsilon \,,$$
$$W_V = 0.22E - 3.8 \,, \qquad (1)$$
$$W_{SF}(_n^p) = 12.1 - 0.25E \pm W_1\epsilon \,,$$

with $r_R = 1.2$ fm, $a_R = 0.674$ fm, $r_I = 1.17$ fm, $a_I = 0.73 + 0.7\epsilon$ fm, $V_{s.o.} = 6.69$ MeV, $r_{s.o.} = 0.89$ fm, $a_{s.o.} = 0.668$ fm, $\epsilon = (N-Z)/A$, $V_1 = 17.7$ MeV, and $W_1 = 9.65$ MeV.

The notation is the same as that of BG, V_R is the real volume, W_V is the imaginary volume, and W_{SF} is the imaginary surface potential, all given in MeV. The Coulomb potential is that of a uniformly charged sphere of radius $R_C = 1.25\ A^{1/3}$. The volume potentials both have Saxon-Woods forms, the surface absorption is a derivative Saxon form with maximum depth equal to W_{SF}, and the spin-orbit potential has the usual derivative

form divided by r. The plus (minus) sign is for proton (neutron) scattering, and the energy E is evaluated, for a given nuclear transition, at the incident projectile energy $E_{\rm lab}$ plus the Q value, taking the center-of-mass transformation into account (not shown explicitly here) for that transition. Thus $E=E_{\rm lab}$ for the ground-state, $E=E_{\rm lab}-Q_{pn}$ for the IAS, $E=E_{\rm lab}-Q(2_1^+)$ for the 2_1^+ state, and $E=E_{\rm lab}-Q(2_1^+)-Q_{pn}$ for the 2_1^+ excited analog state (EAS), and similarly for the two-phonon states treated in this paper. The only Coulomb correction to the proton energy is in the real volume potential, where $z=1$ for protons and 0 for neutrons.

The proton potentials given by Eq. (1) are the same as those given by the BG "best fit" on the average over the Pd isotopes. The resulting neutron potentials are determined by the use of the MSU (p,n) potential to adjust the Lane term. See the Appendix for more detail on how this "regional" optical potential is obtained.

The optical potential of Eq. (1) was developed by adjusting it to 22 MeV proton data,[8] where it works equally well over the Pd isotopes. As can be seen in this paper, it also works remarkably well for the 26 MeV Pd (p,p') data[9] and the 26 MeV Pd (p,n) data. We emphasize that Eq. (1) gives a common "regional" optical potential for the Pd isotopes, and no adjustments of the optical-potential parameters were made for individual isotopes or for different energies except for the systematic dependencies on energy, mass number, and isospin already included in Eq. (1). As such, it is not expected to provide a detailed fit to all the data but rather to provide a model for examining isospin conservation and symmetry in the scattering on a set of isotopes by an isospin complete set of nucleons.

As discussed in the Appendix, unlike Ref. 17, there is no explicit energy dependence in the W_1 term. The difference of including the W_1 energy dependence explicitly throughout our potential would be in the imaginary surface term for neutrons. The imaginary surface term for protons is designed, on the average, to be adjusted back to the modified BG value and is therefore almost unaffected by our choice. Pd(n,n) measurements, including the study of energy dependence, would be of considerable interest in examining the question of the energy-dependent imaginary isospin term in the global optical potential.

Since the imaginary part of the optical potential accounts for flux absorbed out of the elastic channel and the full coupled-channels calculations (CC) include some of this coupling explicitly, the imaginary part of the coupled-channels optical potentials is reduced compared to the elastic scattering values. Our procedure has been to decrease the imaginary optical potentials by 15% in each channel. This value was determined by comparing elastic and inelastic [distorted-wave Born approximation (DWBA) and CC] calculations versus data with corresponding variations in deformation parameters and imaginary optical-potential reductions.

B. Ten-channels analysis: Collective-model deformation parameters

In this section we present the results of coupled-channel calculations for the ^{104,106,108,110}Pd isotopes and compare with (p,n), (p,p), and (p,p') data. In the present calculations, full coupling includes ten channels, the ground state, the 2_1^+ one-phonon state, the $0_2^+,2_2^+,4_1^+$ two-phonon states and all of their analogs. The coupling form factors are taken from the collective model. The deformation parameters β are presented in Table III. The

TABLE III. Deformation parameters. The nuclear deformation parameter $\delta=\beta R$ is the appropriate quantity for comparing different probes, but in this case all radii are $1.2\,A^{1/3}$, so that β's are equally appropriate.

		Empirical (coupled-channels)			Empirical (measured)	Schematic model		
Isotope	Transition	$\beta_{pp'}$	$\beta_{nn'}$	β_1	$\beta_{\rm em}$	$\beta_{pp'}$	$\beta_{nn'}$	$\beta_{\rm em}$
^{104}Pd	$0_1^+\rightarrow 2_1^+$	0.18	0.17	0.263	0.209	0.199	0.188	0.182
	$2_1^+\rightarrow 4_1^+$	0.10	0.10	0.10				
	$2_1^+\rightarrow 2_2^+$	0.18	0.18	0.18				
	$2_1^+\rightarrow 0_2^+$	0.10	0.10	0.10				
	$0_1^+\rightarrow 2_2^+$	0.025	0.025	0.025				
^{106}Pd	$0_1^+\rightarrow 2_2^+$	0.19	0.18	0.265	0.229	0.209	0.195	0.192
	$2_1^+\rightarrow 4_1^+$	0.114	0.114	0.114				
	$2_1^+\rightarrow 2_2^+$	0.20	0.20	0.20				
	$2_1^+\rightarrow 0_2^+$	0.10	0.10	0.10				
^{108}Pd	$0_1^+\rightarrow 2_1^+$	0.21	0.20	0.277	0.243	0.225	0.214	0.208
	$2_1^+\rightarrow 4_1^+$	0.124	0.124	0.124				
	$2_1^+\rightarrow 2_2^+$	0.19	0.19	0.190				
	$2_1^+\rightarrow 0_2^+$	0.10	0.10	0.10				
^{110}Pd	$0_1^+\rightarrow 2_1^+$	0.22	0.209	0.275	0.257	0.237	0.227	0.222
	$2_1^+\rightarrow 4_1^+$	0.15	0.15	0.15				
	$2_1^+\rightarrow 2_2^+$	0.23	0.23	0.23				
	$2_1^+\rightarrow 0_2^+$	0.13	0.13	0.13				

values of $\beta_{pp'}$ have been adjusted in the coupled-channels calculation to fit the (p,p') data of Ref. 9. For the 2_1^+ transition, β_{nn}, is scaled from the empirical β_{pp}, using the isovector deformation parameter β_1 from an open-shell random-phase approximation (RPA) schematic model[18] for neutron-excess nuclei, which treats both the $0\hbar\omega$ space (including pairing) and the $2\hbar\omega$ giant-quadrupole space (core polarization). The trend of the empirical and schematic-model β's is that the Pd isotopes become more collective as the number of neutrons towards the middle of the filling shell is increased.

The excitation of the 2_1^+ analog is primarily a two-step process,[7] and for energies in the range we are studying here, the excited-analog cross sections are fairly insensitive to the one-step amplitudes, especially in the case of positive β_1, such as are expected for the Pd isotopes. In an earlier paper[19] on ^{54,56}Fe, there were (n,n), (p,p), and (p,n) elastic and inelastic data, and the (p,n) data were at 35 MeV, where the one step to the 2^+ excited analog is more prominent. The primary difference, however, is that for ^{54}Fe the β_1 is large and negative compared to the isocalar deformation parameter β_0, and because of this, the one- and two-step amplitudes are more comparable and interfere somewhat constructively. Consequently, it was possible to establish β_1 empirically, and in that case the agreement between theory and experiment was remarkably good.

The β's for the one-phonon to the three two-phonon transitions in the Pd isotopes were adjusted to the (p,p') data, where available. In the harmonic vibrator model these β's should all be the same as those in the transition from the ground to the 2_1^+ state. It can be seen from Table III that for a given isotope these β's are all different and are either roughly equal to or less than those for the ground to the 2_1^+ transition, implying phonon mixing or fractionation. However, in the case of ^{104}Pd, the (p,p') excitation of the two-phonon 2_2^+ required β's for the second step that were larger than for the first step. In order to explain this large coupling, it was necessary to include a one-step amplitude from the ground to the 2_2^+ two-phonon state. However, the calculation of the (p,p') differential cross section including this phonon mixing compared with data could not distinguish that a one-step was needed. The experimental (p,n) two-phonon transition could not be resolved, and there are no Pd(n,n') data, so for lack of empirical information the two-phonon β's for a given multipolarity were taken as common for all nuclear probes, which is equivalent to taking $\beta_1=\beta_0$.

The empirical $\beta_{pp'}$'s shown in Table III, which have been determined in the present work, are smaller than the empirical electromagnetic (em) β's for the 2_1^+ transitions taken from Raman *et al.*[20] The schematic model[18] predicts $\beta_{pp'}$ greater than β_{em} for these nuclei. This is due to the valence neutrons being more free to vibrate than the valence protons in the Pd isotopes and to the fact that a proton probe sees primarily neutrons (i.e., V_{np} is approximately $3V_{pp}$ in this energy range), while the em interaction is sensitive only to the nuclear protons. The $\beta_{pp'}$'s could be larger if the two-phonon β's were all larger. This is because the interference between the one- and three-step (via the two-phonon states and back) amplitudes to the 2_1^+ is destructive. One could take the point of view that the two-phonon states are fractionated, and the remaining strength is in states undetected in the (p,p') experiments, which nevertheless contribute to the multistep excitation of the 2_1^+ state. The maximum effects based on the uniform collective model can be calculated by setting all the β's equal (and determining how much the β for the 2_1^+ has to be increased to fit the (p,p') data. This was done for the most collective of this set of isotopes ^{110}Pd: the value determined was $0.23 \leq \beta_{pp'} \leq 0.25$, which is somewhat larger than the schematic-model prediction for $\beta_{pp'}$. However, the empirical β_{em} is still larger than the empirical $\beta_{pp'}$, and this is disturbing since the relative trends of the β's with probe and isotope from the schematic model are expected to be more reliable than the absolute values.

The absolute values of the β_{em} was established by placing the sum-rule strength of the $0\hbar\omega$ proton multipole matrix element, M_p $[B(E2)=|M_p|^2]$ at the 2_1^+ experimental energy, and then taking the $2\hbar\omega$ core-polarization effects into account. This procedure, within the schematic-model assumptions, is expected to give an upper limit on β_{em}. The absolute values of the β_{em}'s from the schematic model are 15 to 20% smaller than the empirical values, while the schematic-model $\beta_{pp'}$'s are about 10% larger than the empirical ones. (The equal β's coupled-channels effect discussed earlier would decrease the discrepancy.) Precise measurements of β_{em} such as can be obtained in electron scattering would be useful in this regard.

Pd(n,n') measurements would also be of considerable interest in determining the $\beta_{nn'}$'s which are expected to be close to the β_{em}'s from our model calculations. In a recent study[21] of the Zr(n,n') isotopes, values of $\beta_{nn'}$ were obtained that were very much in agreement with the open-shell schematic model,[18] while measured β_{em}'s for the Zr isotopes[20] are at odds with what is expected from the schematic model. Accurate determinations of β_{em} from (e,e') would also be of interest.

C. Coupled-channels results compared to data

Calculations with ten coupled-channels described above with the Oregon State/LLNL coupled-channels code[22] are presented in this section. The theoretical and experimental integrated cross sections for (p,n) for the ^{104,106,108,110}Pd isotopes for protons at 26 MeV are presented in Tables I and II.

The calculated ^{108}Pd(p,p) elastic ratio to Rutherford and the inelastic 2_1^+, 2_2^+, 4_1^+, and 0_2^+ differential cross sections are shown in Fig. 7 compared to the data of Lindstroem *et al.*[9] at 25.9 MeV. The two-phonon 0^+ and 4^+ cross sections are unresolved; the theoretical results include the separate contributions and the sum. Calculated ^{108}Pd(p,n) ground-state analog, first excited state (2_1^+) analog, and two-phonon triplet $(0_2^+,2_2^+,4_1^+)$ analog differential cross sections are shown in Fig. 8 compared with the data from the present experiment. The two-phonon $0_2^+,2_2^+$, and 4_1^+ cross sections are unresolved

for our experimental data; the theoretical results include the separate contributions and the sum.

The (p,n) experimental results at $E_p = 26$ MeV from the present work are presented in Figs. 4–6. The calculated and experimental differential cross sections for the ^{104,106,108,110}Pd$(p,n)0^+$ ground-state isobaric analog are shown in Fig. 4. The cross sections for the ^{104,106,108,110}Pd$(p,n)2_1^+$ excited-analog state are shown in Fig. 5. The cross sections for the ^{104,106,108,110}Pd(p,n) unresolved two-phonon triplets $(2_2^+ + 4_1^+ + 0_2^+)$ are shown in Fig. 6; the theoretical results are given as the sum of the three separate contributions.

Variations of up to 50% in $\sigma/(N-Z)$ for the isobaric analog state have been observed and explained for a number of different isotope sets, e.g., ^{92,98,100}Mo (Ref. 7), ^{76,80,82}Se (Ref. 5), ^{144,148,150,152}Sm (Ref. 4), ^{46,48,50}Ti (Ref. 23), ^{54,56}Fe (Ref. 19), and most recently, ^{90,92,94}Zr (Ref. 3). Coupled-channels calculations are in good agreement with the experimental analog cross sections, and the effect has been explained[7] as due to the contribution of three three-step processes, which all interfere destructively with the dominant one-step process. The calculations involve a full coupled-channels treatment to all orders, but a description based[7] on a perturbation expansion involving intermediate Green's functions is adequate to explain the effect. The three-step processes involve products of the charge-exchange amplitude times the product of two inelastic amplitudes. The three amplitude routes to the IAS (shown in Fig. 9), are 0^+ g.s. $(p,p')2_1^+(p,n)2_1^+(n,n')$ IAS, 0^+ g.s. $(p,p')2_1^+(p,p')0^+$ g.s. (p,n) IAS, and 0^+ g.s. (p,n) IAS $(n,n')2_1^+(n,n')$ IAS, where the inelastic routes involve excitation or deexcitation accordingly. The amount that the IAS is reduced by this destructive three-step interference varies

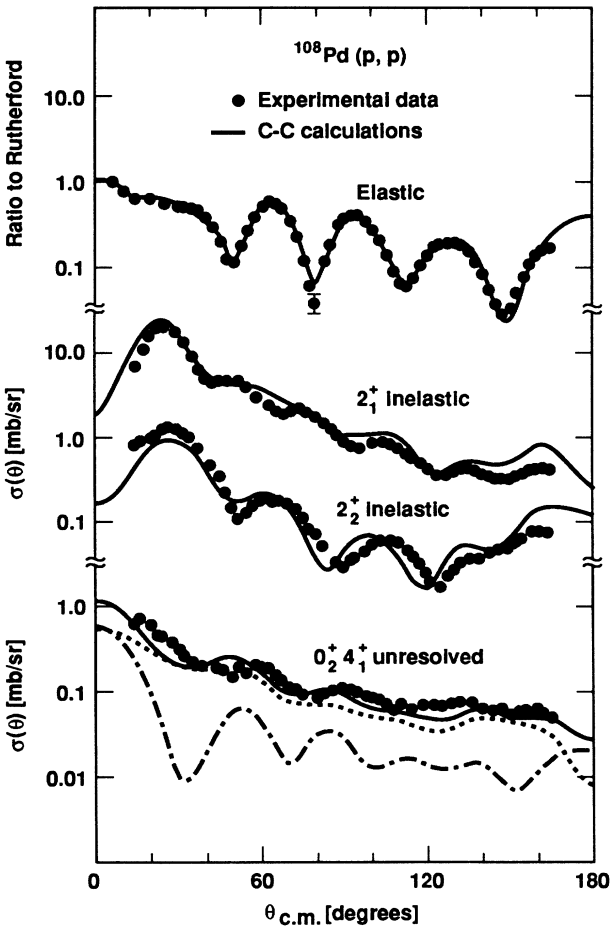

FIG. 7. The ^{108}Pd(p,p) elastic ratio to Rutherford and the inelastic 2_1^+, 2_2^+, 4_1^+, and 0_2^+ differential cross sections. The experimental data are by Lindstroem *et al.* (Ref. 9), the curves represent the coupled-channels calculations. The two-phonon 0_2^+ and 4_1^+ states were not resolved in the experiment; the theoretical curves show the separate contributions from the 0_2^+ level (dashed-dotted curve) and the 4_1^+ level (dotted curve) and the sum of both (solid curve).

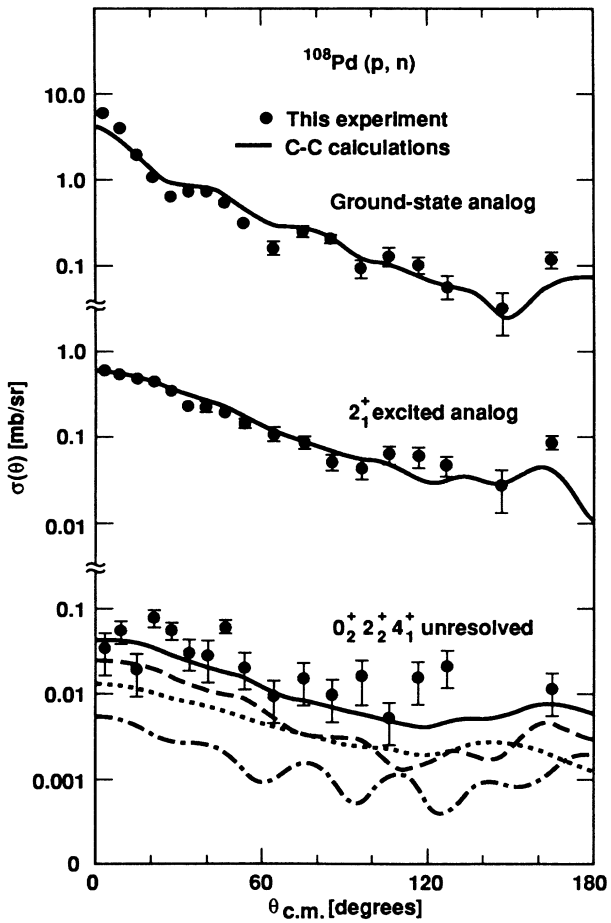

FIG. 8. The ^{108}Pd(p,n) ground-state analog, first excited-state (2_1^+) analog, and two-phonon triplet $(0_2^+, 2_2^+, 4_1^+)$ analog differential cross sections. The experimental data are from this experiment, the curves represent the coupled-channels calculations. The two-phonon triplet was not resolved in the experiment; the theoretical curves show the separate contributions from the 0_2^+ analog state (dashed-dotted curve), the 2_2^+ analog state (dashed curves), the 4_1^+ analog state (dotted curve), and the sum of all three (solid curve).

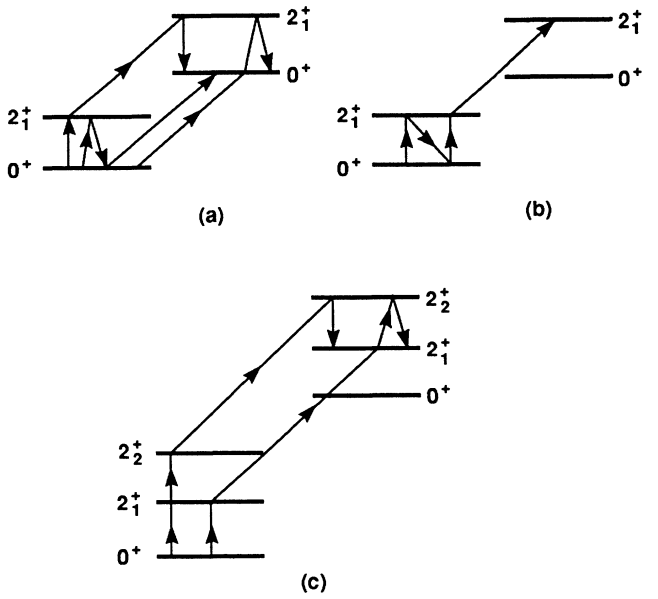

FIG. 9. Multistep processes that interfere destructively with the one-step analog transition, with the two-step excited analog one-phonon transition, and four-step transitions that interfere with the two-step excited analog two-phonon transitions.

with the collectivity of the isotope. Similar three-step interference effects, involving intermediate collective states such as the 3_1^- or the giant resonances, which are more uniform from isotope to isotope, also exist but would not contribute to an isotope effect.

Figure 10 shows the reduced total IAS cross section $\sigma/(N-Z)$ versus $\beta_{pp'}^2$ for ^{92,94,98,100}Mo at E_p of 26 MeV, ^{90,92,94}Zr at 25 MeV, and from the present work ^{104,106,108,110}Pd at 26 MeV. $\sigma/(N-Z)$ is expected to change with A only about 10% on the basis of DWBA calculations. The coupled-channels calculations shown as a solid line in Fig. 10 follow the downward trend of the data with β^2 corresponding to increased collectivity. The coupled-channels calculations agree quite well with the data for the Pd and Mo isotopes. One might expect that not only the relative trend but even the absolute values of $\sigma/(N-Z)$ and β^2 might be closer than we see in Fig. 10 for Mo and Pd. To examine this question further, a coupled-channels calculation for ^{100}Mo has been performed using the regional optical potentials developed and utilized in this paper. In addition to the (p,n) data[7] at 26 MeV, there are also (p,p) data[24] at 25.6 MeV. Of the three Mo isotopes in Fig. 9, only ^{100}Mo(p,p) was measured. The agreement of the coupled-channels calculations with the (p,n) data to the ground-state IAS and the 2_1^+ IAS, and the proton elastic scattering and inelastic scattering data to the 2_1^+ and the two-phonon triplet (0_2^+, 2_2^+, and 4_1^+) are of the same quality as one sees in this paper for the Pd isotopes.

The main difference is that the $\beta_{pp'}$ from the ground-state to the 2_1^+ state in ^{100}Mo is 0.205 in the present work compared to 0.226 in the earlier work.[7] The schematic-model value is also 0.226. The value of $\beta_{pp'}$ needed in the coupled-channels calculations compared to data is therefore about 10% smaller than the schematic-model value, consistent with the results in Table III for the Pd isotopes. The results can be compared to those of ^{104}Pd since the energies of the 2_1^+ states are comparable in the two cases. The $\beta_{pp'}$ for ^{104}Pd is smaller than that of ^{100}Mo. Both isotopes have the same number of neutrons outside the closed shell of 50 nucleons, but ^{100}Mo has eight proton holes compared to only four in ^{104}Pd. The coupled-channels recalculation of $\sigma/(N-Z)$ for the IAS using the current regional optical potential and the $\beta_{pp'}$'s obtained from comparison to the data of Ref. 24 is plotted in Fig. 10; the agreement with data[7] is of the same quality as that for Pd. However, note that the curve for Mo now lies much closer to the curve for Pd (see the points in parentheses in Fig. 10).

The integrated cross section listed in Table IV and the angular distributions in Fig. 11 show data and full coupled-channels calculations compared with the one- and two-step contributions to the reactions ^{108}Pd$(p,n)2_1^+$ and ^{108}Pd$(p,p')2_2^+$. These are both predominantly two-step processes. The inelastic excitation of the 2_2^+ two-phonon state is a two-step excitation within the harmonic-vibrator model. Since we do not introduce a direct excitation of the 2_2^+ from the ground state, the two-step angular distribution in Fig. 11 is a direct excita-

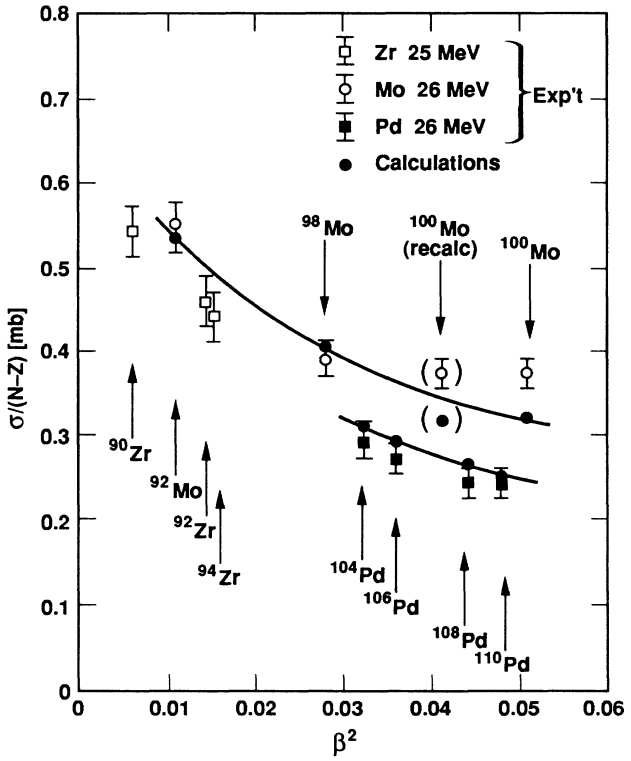

FIG. 10. Total reduced cross section $\sigma/(N-Z)$ as a function of β_2^2 showing the effect of the variation in the deformation parameter β_2 on the ground-state analog cross section. The zirconium data are from Anderson *et al.* (Ref. 3) and the molybdenum data and calculations are from Madsen *et al.* (Ref. 7).

TABLE IV. Comparison of experimental and calculated cross sections in mb for ^{108}Pd.

Target isotope	Source	Cross sections $(p,n)0_1^+$	$(p,n)2_1^+$	$(p,p')2_2^+$
^{108}Pd	Experiment	3.78±0.26	1.31±0.10	2.5±0.1
	Full Coupl.	4.26	1.33	2.04
	Two Step		1.39	
	One Step	6.03	0.082	1.01[a]

[a]Corresponds to the value of $\beta_{pp'}$ (g.s.$\rightarrow 2_2^+$) of 0.033.

tion from the ground state, which was not included in Fig. 7. The value of $\beta_{pp'}$ (g.s.$\rightarrow 2_2^+$) for the one step of Fig. 11 is 0.033. This value combined with $\beta_{pp'}$ $(2_1^+ \rightarrow 2_2^+)=0.098$ gives almost as good an angular distribution for the ^{108}Pd(p,p') 2_2^+ cross section as is given by the pure two step of Fig. 7. The excitation of the 2_1^+ analog is also primarily a two-step process,[7] and except for special cases,[19] the excited-analog cross sections are fairly insensitive to the one-step amplitudes. It is interesting to note that the two step is more diffractive in the inelastic case in agreement with experiment, unlike the 2_1^+ analog excitation, which is somewhat washed out compared to the one-step contribution, also in agreement with experiment. The primary difference is that the form factors for the inelastic case emphasize the surface somewhat more than in the (p,n) case. The fact that the coupled-channels calculations are in good agreement with angular distribution diffraction patterns is rather striking confirmation of our understanding of these multiple-step effects within the collective model.

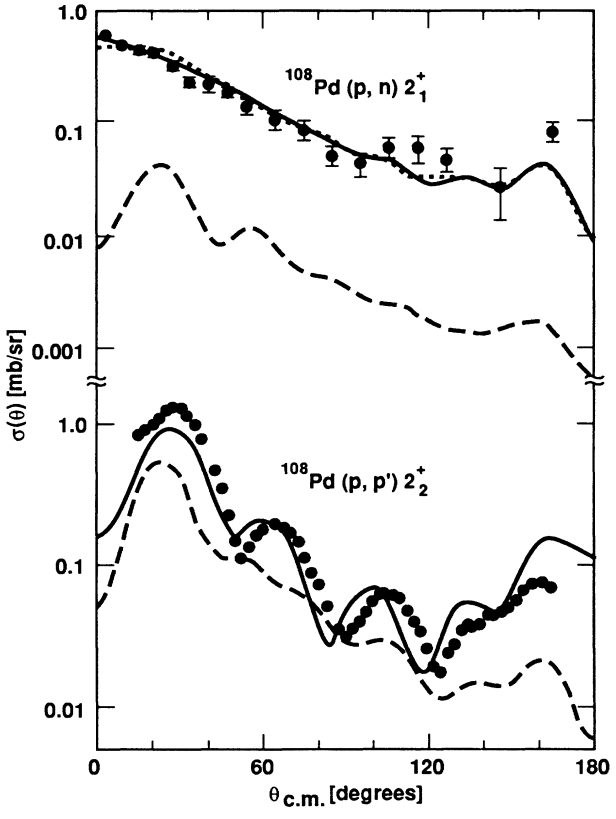

FIG. 11. The full coupled-channels calculations (solid curve) are compared to the $(p,n)2_1^+$ experimental data and to the $(p,p')2_2^+$ experimental data. The individual contributions of the one-step process (dashed curve) and the two-step process (dotted curve) are also shown.

As seen in Fig. 3, the resolution of the two-phonon states in (p,n) is not adequate to help sort out the various contributions from these states. Further studies of Pd(p,p') and Pd(n,n') measurements would be valuable. Ideally em decay rates are needed to determine the one-step proton deformation parameters. A study of the literature on such measurements revealed a wide variety of disagreeing rates and, therefore, $\beta_{\rm em}$'s for the transitions of interest. The understanding of these isospin nuclear structure effects benefits greatly from measurements with a wide variety of probes.

IV. SUMMARY AND DISCUSSION

We have measured the (p,n) reaction to the 0_1^+, 2_1^+, and unresolved 0_2^+, 2_2^+, and 4_1^+ analog states in the even palladium isotopes with 26 MeV protons. As in previous cases, the ground-state analog and the 2_1^+ analog cross sections show strong collective effects. Coupled-channels calculations have been performed using a modification of the MSU version of the Becchetti-Greenless optical potential to make it consistent with potentials obtained from searches in the Pd isotopes.

According to the Lane model, for ground-state analogs the cross section is proportional to neutron excess. Our results shown in Fig. 10, and in previous publications, have shown that there are strong deviations from that simple proportionality. A comparison with coupled-channels equations has clearly established that this effect is due to three-step amplitudes which interfere destructively with the dominant first-order Lane-model result. The strength of these destructive terms is proportional to the inelastic cross section, so the magnitude of this effect depends on the collectivity of the nucleus. These higher-order amplitudes can reduce the cross section by as much as 50% compared to a first-order (DWBA) calculation.

As discussed in Sec. III C, the agreement of the coupled-channels calculations, using the current regional optical potential and the $\beta_{pp'}$'s obtained from comparison to the data for ^{100}Mo(p,p') is of the same quality as the

earlier results.[7] Of the three Mo isotopes plotted in Fig. 10, only ^{100}Mo(p,p') is measured[24] at 26 MeV. The indication from this one calculated point for ^{100}Mo is that the coupled-channels curve for Mo would lie much closer to the curve for Pd. This would make the plot for $\sigma/(N-Z)$ versus β^2 more universal for a given mass region in that not only the relative trend, but even the absolute values of $\sigma/(N-Z)$ and β^2 would lie closer than we see in Fig. 10 for Mo, Zr, and Pd. Elastic and inelastic proton scattering measurements on ^{92,98}Mo and ^{90,92,94}Zr at 26 MeV are needed to investigate, with the current regional optical potential, the universality for all three sets of isotopes.

The 15% reduction in the imaginary potentials has been chosen to account for the explicit channels included in the coupled-channels calculations. If the amount of reduction were decreased, the inelastic cross sections could be compensated for by increasing β; however, the elastic cross section could not be compensated in this way because increasing the imaginary potential and increasing β both decrease the elastic scattering. The amount of freedom one has to adjust the parameters within these opposing effects is limited by the experimental errors. The ground-state analog cross sections plotted in Fig. 10 would increase with a smaller reduction (e.g., 8%) in the imaginary potential and decrease with the compensating inelastic increase in β (three-step interference). These effects are compensating, but because the analog cross section depends on the elastic and inelastic cross sections, there is an underlying constraint on the results of Fig. 10, based on the accuracy of the elastic, inelastic, and analog data. The 15% has been adjusted to the elastic and inelastic scattering over the isotopes; within the error bars a reduction as low as 8% would have acceptable quality in comparison to all the data. The inelastic β's would have to increase about 4% in that case, with the corresponding shift in the abscissa of Fig. 10. On the other hand, a different regional optical potential could have somewhat larger changes in the values of β and V_1 as was the case for the ^{100}Mo recalculation with the present optical potential. This question could be addressed rather precisely with a full set of data including elastic and inelastic neutron measurements on these isotopes.

The charge-exchange transition to analogs of the 2_1^+ collective vibrational states in principle provide a means of measuring the isovector deformation parameter β_1. The present study confirms, however, that in this energy range extractions of β_1 can be made only in special cases. As discussed in Sec. III B, second-order effects, which are large in the 20 MeV range, totally dominate these excited-analog transitions. Only in the case where β_1 is negative, is such an extraction possible. As discussed in Sec. III B, such a case is the nucleus ^{54}Fe, analyzed in an earlier publication. In the case of Pd the β_1 parameters are expected to be positive with the consequence that differences in differential cross section with and without the inclusion of the one-step process were not significant in comparison with the data. It would be interesting to make measurements in the 60–100 MeV range, an energy range high enough that the multistep amplitudes are relatively weak but not so high that the pure charge-exchange interaction becomes too small to obtain accurate enough data. Even at these energies, however, the two-step amplitudes would be large enough that coupled-channels calculations would still have to be done in order to make meaningful extractions of the isovector deformation parameters. This seeming difficulty can actually be an advantage because of the phase information which one can determine from the interference of the first- and second-order amplitudes.

The deformation parameters $\beta_{pp'}$ extracted from our analysis of Pd(p,p') scattering are about equal to the electromagnetic values from the literature. As explained in Sec. III B, this is considered disagreement, since on the basis of shell structure the quadrupole vibrational amplitude of nuclear neutrons is expected to be larger than that of the protons. A schematic-model RPA calculation of the deformation parameter is in quite good agreement with the $\beta_{pp'}$ values that have been extracted. Inelastic neutron scattering measurements are needed to clear up the uncertainties on the isospin structure of the quadrupole vibrational state in palladium.

ACKNOWLEDGMENTS

The authors thank Dr. V. Riech and co-workers for making their elastic and inelastic proton scattering results for Pd available in tabular form prior to publication. This work was performed under the auspices of the U.S. Department of Energy by the Lawrence Livermore National Laboratory under Contract No. W-7405-ENG-48, and was also supported at the University of Hamburg by the German Federal Ministry of Research and Technology (BMFT) under Contract No. 06-HH-175.

APPENDIX: PROCEDURE FOR OBTAINING REGIONAL OPTICAL PARAMETERS

The following procedure was adopted for determining our regional Lane potentials. Starting with the Becchetti-Greenlees (BG) "'best-fit"[16] proton potentials, adjustments were made to obtain a good global fit to the 22 MeV Pd(p,p) data of Aoki *et al.*[8] The parameters were adjusted from BG values in the direction of those used in Ref. 8, with a significant improvement over the BG calculations in the ratio to Rutherford cross sections for Pd. The radii, diffusenesses, and spin-orbit parameters deviate noticeably from the BG values. The values of the parameters for Pd isotopes might be expected to deviate from BG values, which concentrated on spherical nuclei. Our adjustments were guided by the work of Ref. 8 and are not intended to represent a "best fit." Nevertheless, good agreement for the inelastic scattering was also calculated for the 22 MeV Aoki proton data using our global optical potentials. The MSU (p,n) potential,[17] without explicit energy dependence in the imaginary component, was used for the isovector part of the potential. The isoscalar term was then modified so that the resulting Lane potential reproduced (on the average for the Pd isotopes) the modified BG potential for protons. The resulting regional Lane optical potential for protons and neutrons, equivalent to Eq. (1), is

$$V_R\left(\begin{matrix}p\\n\end{matrix}\right)=52.5-0.32E+\bar{\epsilon}(24.0-V_1)+0.4zZ/A\pm V_1\epsilon\ ,$$
$$W_V=0.22E-3.8\ , \tag{A1}$$
$$W_{\rm SF}\left(\begin{matrix}p\\n\end{matrix}\right)=11.8-0.25E+\bar{\epsilon}(12.0-W_1)\pm W_1\epsilon\ ,$$

where $r_R=1.22$ fm, $a_R=0.674$ fm, $r_I=1.17$ fm, $a_I=(0.73+0.7\epsilon)$ fm, $V_{\rm s.o.}=6.69$ MeV, $r_{\rm s.o.}=0.89$ fm, $a_{\rm s.o.}=0.668$ fm, and $\epsilon=(N-Z)/A$. In Eq. (A1) $\bar{\epsilon}$, which is used to adjust the proton potentials to the modified BG values, is taken as 0.14 and is the average over the isotopes. The notation is the same as that of BG as used in Eq. (1). The MSU (p,n) potential[8] is given by

$$V_R(p,n)=\frac{2(N-Z)^{1/2}}{A}V_1\ ,$$
$$W_{\rm SF}(p,n)=\frac{2(N-Z)^{1/2}}{A}(W_1-0.31\bar{E})\ , \tag{A2}$$

where

$$\bar{E}=(E_p+E_n)/2=E_{\rm lab}-Q_{pn}/2\ . \tag{A3}$$

The MSU (p,n) potential has an energy dependence in the imaginary part. The "regional" optical potentials of Eqs. (A1) and (1) do not have explicit energy dependence in the W_1 term. The Lane potentials used in this work are given by $V_1=17.7$ MeV (Ref. 25) and $W_1=9.65$ MeV, where the geometry is the same as Eq. (A1). This value of $W1$, which has been adjusted to fit the 26 MeV (p,n) data, takes the energy dependence of the MSU potential into account by adjusting it downward from 17.7 MeV by a term proportional to $E_{pn}=(E_p+E_n)/2=E_{\rm lab}-Q_{pn}/2$. The value of 9.65 used here corresponds to a proportionality in the energy dependence of 0.41 as compared to the 0.31 used in the MSU potential. The optical potentials used for the 22 MeV proton scattering comparisons were evaluated using Eq. (A2) with $W_1=11.4$, which corresponds to the same energy-dependent proportionality of 0.41 in the isospin term. By eliminating the explicit energy dependence of W_1 in Eq. (A1), we have avoided the necessity of an imaginary Coulomb correction, which would be needed with the MSU potential to make it globally isospin consistent.

[1]C. H. Poppe, S. M. Grimes, J. D. Anderson, J. C. Davis, W. H. Dunlop, and C. Wong, Phys. Rev. Lett. **33**, 856 (1974).

[2]S. M. Grimes, C. H. Poppe, J. D. Anderson, J. C. Davis, W. H. Dunlop, and C. Wong, Phys. Rev. C **11**, 158 (1975).

[3]J. D. Anderson, R. W. Bauer, V. R. Brown, S. M. Grimes, V. A. Madsen, B. A. Pohl, C. H. Poppe, and W. Scobel, Phys. Rev. C **38**, 1601 (1988).

[4]C. Wong, V. R. Brown, V. A. Madsen, and S. M. Grimes, Phys. Rev. C **20**, 59 (1979).

[5]C. Wong, S. M. Grimes, C. H. Poppe, V. R. Brown, and V. A. Madsen, Phys. Rev. C **26**, 889 (1982).

[6]A. M. Lane, Phys. Rev. Lett. **8**, 171 (1962); Nucl. Phys. **35**, 676 (1962).

[7]V. A. Madsen, V. R. Brown, S. M. Grimes, C. H. Poppe, J. D. Anderson, J. C. Davis, and C. Wong, Phys. Rev. C **13**, 548 (1976).

[8]Y. Aoki, H. Iida, K. Hashimoto, K. Nagano, M. Takei, Y. Toba, and K. Yagi, Nucl. Phys. **394**, 41 (1983).

[9]V. Riech, E. Fretwurst, G. Lindstroem, K. F. Von Reden, R. Scherwinski, and H. P. Blok, Phys. Lett. B **178**, 10 (1986); G. Lindstroem *et al.* (unpublished); V. Riech, private communication.

[10]Y. Holler, A. Kaminsky, B. Scharlemann, H. Krause, R. Langkau, W. Peters, G. Poppe, N. Schirm, W. Scobel, and R. Wien, Nucl. Instrum. Methods A **235**, 123 (1985).

[11]E. Mordhorst, M. Trabandt, A. Kaminsky, H. Krause, and W. Scobel, Phys. Rev. C **34**, 103 (1986).

[12]A. Kaminsky, Y. Holler, and W. Scobel, Nucl. Instrum. Methods A **244**, 443 (1986).

[13]We are indebted to D. Hilscher for the Pd-7 units. See also, W. P. Zank, D. Hilscher, G. Ingold, U. Jahnke, M. Lehmann, and H. Rossner, Phys. Rev. C **33**, 519 (1986).

[14]G. Dietze and H. Klein, Report No. ND-22 der PTB Braunschweig, 1982.

[15]W. Stoeffl, private communication.

[16]F. D. Becchetti and G. W. Greenless, Phys. Rev. **182**, 1190 (1969).

[17]D. M. Patterson, R. R. Doering, and A. Galonsky, Nucl. Phys. **A263**, 261 (1976).

[18]V. A. Madsen and V. R. Brown, Phys. Rev. Lett. **52**, 176 (1984).

[19]R. D. Smith, V. R. Brown, and V. A. Madsen, Phys. Rev. C **33**, 847 (1986).

[20]S. Raman, C. H. Malarkey, W. T. Milner, C. W. Nester, Jr., and P. H. Stelson, At. Data Nucl. Data Tables **36**, 21-22 (1987).

[21]Y. Wang and J. Rapaport, Z. Phys. A **331**, 305 (1988).

[22]M. J. Stomp, F. A. Schmittroth, and V. A. Madsen, USAEC Technical Report No. AT(45-1)-222, 1968 (unpublished). Revisions and additional features are included in the current LLNL version of this code.

[23]V. R. Brown, C. Wong, C. H. Poppe, J. D. Anderson, J. C. Davis, S. M. Grimes, and V. A. Madsen, Phys. Rev. C **33**, 1235 (1986).

[24]E. Fretwurst, B. Lindstroem, K. F. Von Reden, V. Riech, S. I. Vasiljev, P. P. Zarubin, O. M. Knyazkov, and I. N. Kuchtina, Nucl. Phys. **A468**, 247 (1987).

[25]The value of 17.7 MeV is used here instead of the 18.8 MeV value of Ref. 17. This is to compensate for the difference in how the energy of the analog state is determined. The empirical value, which is closer to $Q_{pn}=1.25\langle Z\rangle A^{1/3}$, is used in the present work, whereas the MSU (p,n) potential uses $Q_{pn}=0.84\langle Z\rangle/A^{1/3}$ (MeV).